Magnetically induced helical textures in superfluid ^{3}He-A

Alexander L. Fetter
Institute of Theoretical Physics, Department of Physics, Stanford University, Stanford, California 94305

Mark R. Williams
Shell Development Company, Bellaire Research Center, P.O. Box 481, Houston, Texas 77001
(Received 6 October 1980)

Bulk ^{3}He-A in a uniform relative superflow is known to deform with increasing parallel magnetic field from a uniform structure to a helical one. This latter texture becomes unstable at a critical field, beyond which the system exhibits runaway nonlinear growth. Subsequent behavior depends on the specific external configuration. In a torus, the texture apparently evolves into a stable wide-angle helix with a reversed and largely quenched superflow. In an applied heat flow, the texture instead oscillates periodically but anharmonically.

I. INTRODUCTION

The evolution of textures in ^{3}He-A under increased magnetic, hydrodynamic, or thermal stress has recently aroused considerable interest.[1–12] This paper treats one simple example of such configurations: one-dimensional textures in the presence of parallel magnetic field and imposed superflow. The predicted behavior of the system is fascinating, for the structure becomes increasingly complicated with increased magnetic stress. The original stable uniform state distorts into a helical structure with small opening angle, and further stress eventually renders the helix catastropically unstable.[11] Depending on the experimental configuration, this instability may signal either the formation of a wide-angle helix or the onset of an intrinsically time-dependent dissipative texture.

Similar phenomena occur in classical hydrodynamics.[13–16] For example, applied stress can induce Bénard convection rolls in a fluid heated from below and Taylor vortices between differentially rotating cylinders. Further increase in the thermal or hydrodynamic stress induces oscillations in these static convection patterns, ultimately leading to a chaotic state. The possibility of similar behavior associated with the superfluid degrees of freedom in ^{3}He-A is indeed intriguing.

Section II reviews the hydrodynamic model of ^{3}He-A and discusses the specific configuration of superflow and parallel magnetic field. The intrinsic differences between superflow established as persistent current in a torus and as superfluid heat transport receive particular attention. In Sec. III, we discuss the stability of textures with increasing magnetic field, not only allowing the order parameter full freedom in the hydrodynamic approximation but also including temperatures well below T_c. The instability of the uniform state (with $\hat{l} = \hat{d} = \hat{z}$ parallel to the flow and magnetic field) occurs at a *finite* wave number and signals the onset of a helical texture. This texture evolves with increasing magnetic field until it too exhibits an instability at a critical magnetic field.[17] The onset of this latter instability occurs as a catastrophic inverted bifurcation (Sec. IV) that may signal the appearance of an intrinsically time-dependent state. For simplicity, this section treats only the dipole-locked limit, which applies for small relative superflow and magnetic field. The subsequent fate of these one-dimensional textures is inferred from the form of the free energy of the unstable helical states (Sec. V). Distinct and dramatic effects are predicted. For persistent flow in a torus, the instability of the helix probably signals the onset of a dissipative time-dependent state that precesses to the reversed orientation ($\hat{l} = -\hat{z}$) and then ultimately relaxes to a stable wide-angle helix with a reduced and reversed relative superflow. For an external heat flow, the instability instead probably marks the onset of an oscillatory dissipative texture with periodic but anharmonic time dependence.

II. HYDRODYNAMIC MODEL

The hydrodynamic model of ^{3}He-A describes the order parameter at every point in the fluid by a complex orbital vector $\hat{m} + i\hat{n}$ (with $\hat{m} \perp \hat{n}$) and a real spin vector $\hat{d}$. Alternatively, the orbital part of the order parameter may be characterized by a real unit vector $\hat{l} \equiv \hat{m} \times \hat{n}$ and the change in phase $\delta\Phi$ associated with local rotations of $\hat{m}$ and $\hat{n}$ about $\hat{l}$ in moving from $\vec{r}$ to $\vec{r} + \delta\vec{r}$. These new degrees of freedom can vary slowly in space and time. The basic hydrodynamic equations describe the dynamics of $\hat{l}$, Φ, and $\hat{d}$ plus

the usual conservation laws of mass, momentum, and energy. Several authors have exhibited these equations[18,19]; the results are complicated and typically involve numerous phenomenological coefficients that are neither measured experimentally nor evaluated theoretically. Fortunately, the present rather simple configuration does not require the full hydrodynamic model, for physically motivated approximations[20] allow us to simplify the model in conditions of steady flow and applied field.

(1) We assume that the "normal" thermodynamic variables are fixed externally. Thus we take the temperature T, the mass density ρ, and the normal-fluid velocity $\vec{v}_n$ to be uniform and constant. This approximation ignores any effect of the superfluid back on the normal degrees of freedom.

(2) The low-lying excitations of the superfluid corresponding to slow spatial and temporal variations of the order parameter are here investigated with a Landau expansion of the free-energy density through second order in the spatial gradients of the order parameter. Specifically, the hydrodynamic free-energy density f_h^0 in the frame with $\vec{v}_n=0$ is given by[21]

$$f_h^0=\tfrac{1}{2}(\vec{v}_s-\vec{v}_n)\vec{\rho}_s(\vec{v}_s-\vec{v}_n)+(\vec{v}_s-\vec{v}_n)\vec{C}\,\mathrm{curl}\hat{l}+\tfrac{1}{2}K_s(\mathrm{div}\hat{l})^2+\tfrac{1}{2}K_t(\hat{l}\cdot\mathrm{curl}\hat{l})^2+\tfrac{1}{2}K_b(\hat{l}\times\mathrm{curl}\hat{l})^2$$
$$+\tfrac{1}{2}K_1(\hat{l}\cdot\vec{\nabla})\hat{d}_\mu(\hat{l}\cdot\vec{\nabla})\hat{d}_\mu+\tfrac{1}{2}K_2(\hat{l}\times\vec{\nabla}\hat{d}_\mu)\cdot(\hat{l}\times\vec{\nabla}\hat{d}_\mu)-\tfrac{1}{2}(\hat{l}\cdot\hat{d})^2+\tfrac{1}{2}(\vec{H}\cdot\hat{d})^2\ , \tag{1}$$

where $\vec{H}$ is the applied magnetic field and the superfluid velocity is defined as

$$\vec{v}_s=\lim_{\delta\vec{r}\to 0}\frac{\delta\Phi}{\delta\vec{r}}\ . \tag{2}$$

Here a summation over repeated indices is implied, and the tensors $\vec{\rho}_s$ and $\vec{C}$ are defined by

$$(\vec{\rho}_s)_{ij}=\rho_s\delta_{ij}-\rho_0\hat{l}_i\hat{l}_j\ , \tag{3a}$$

$$(\vec{C})_{ij}=C\delta_{ij}-C_0\hat{l}_i\hat{l}_j\ . \tag{3b}$$

The first seven terms in Eq. (1) are the kinetic and elastic contributions, and the corresponding phenomenological parameters have known temperature dependences from model calculations.[3,12,22] The last two terms are the dipole and magnetic contributions, respectively.

(3) It is often preferable to work directly in the laboratory frame, where the corresponding hydrodynamic free-energy density f_h is obtained by a Galilean transformation

$$f_h=f_h^0+\vec{j}^{\,0}\cdot\vec{v}_n+\tfrac{1}{2}\rho v_n^2\ . \tag{4}$$

Here

$$\vec{j}^{\,0}=\vec{\rho}_s(\vec{v}_s-\vec{v}_n)+\vec{C}\,\mathrm{curl}\hat{l} \tag{5}$$

is the current in the frame with $\vec{v}_n=0$. A simple calculation shows that f_h differs from f_h^0 in that the first two terms of Eq. (1) are replaced by $\frac{1}{2}\vec{v}_s\vec{\rho}_s\vec{v}_s+\vec{v}_s\vec{C}\,\mathrm{curl}\hat{l}+\frac{1}{2}\vec{v}_n\vec{\rho}\vec{v}_n$, where $\vec{\rho}_n=\rho\vec{1}-\vec{\rho}_s$ is the normal-fluid density tensor. This function f_h has the natural variables $\vec{v}_s$ and $\vec{j}$, whereas $\vec{v}_s$ and $\vec{v}_n$ often provide a more convenient set. Since $\vec{v}_n$ may be expressed as

$$\vec{v}_n=\frac{\partial f_h}{\partial\vec{j}}\ , \tag{6}$$

a Legendre transformation allows us to introduce the new "free energy"

$$f=f_h-\vec{v}_n\cdot\vec{j}\ , \tag{7}$$

which now depends on the desired variables $\vec{v}_s$ and $\vec{v}_n$. A combination of Eqs. (1), (4), (5), and (7) shows that

$$f=f_h^0-\tfrac{1}{2}\rho v_n^2\ , \tag{8}$$

which serves as our fundamental free-energy density.

(4) We assume that the Cross-Anderson orbital viscosity[23] dominates the dynamical behavior of the order parameter. Thus the dynamical equation for $\hat{l}$ is given by[20]

$$\mu\hat{l}\times\left(\frac{\partial\hat{l}}{\partial t}+\vec{v}_n\cdot\vec{\nabla}\hat{l}\right)=-\hat{l}\times\left(\frac{\delta f}{\delta\hat{l}}\right)_{\delta\Phi=0,\ \delta\hat{d}=0}\ , \tag{9}$$

where μ is a phenomenological "orbital viscosity" that characterizes the relaxation of the quasiparticle distribution when $\hat{l}$ is displaced from its equilibrium orientation. Since changes in the orientation of the spin vector $\hat{d}$ and rotations of $\hat{m}$ and $\hat{n}$ about $\hat{l}$ require no quasiparticle redistribution, $\hat{d}$ and Φ can change instantaneously to minimize the free energy:

$$\hat{d}\times\left(\frac{\delta f}{\delta\hat{d}}\right)_{\delta\hat{l}=0,\,\delta\Phi=0}=0\ , \tag{10}$$

$$\left(\frac{\delta f}{\delta\Phi}\right)_{\delta\hat{l}=0,\,\delta\hat{d}=0}=0\ . \tag{11}$$

Equation (11) guarantees current conservation, for it implies that

$$-\left(\frac{\delta f}{\delta\Phi}\right)_{\delta\hat{l}=0,\,\delta\hat{d}=0}=\vec{\nabla}\cdot\left(\frac{\partial f}{\partial\vec{v}_s}\right)_{\delta\hat{d}=0}=\vec{\nabla}\cdot\vec{j}^{\,0}=0\ , \tag{12}$$

where $\vec{j}^{\,0}$ [see Eq. (5)] can be rewritten in terms of

the supercurrent $\vec{j}_s$ and normal current $\vec{j}_n$ in the laboratory frame as follows

$$\vec{j}^0 = \vec{j}_s + \vec{j}_n - \rho \vec{v}_n \ . \tag{13}$$

Equations (9)–(11) form the basis of our hydrodynamic model. For simplicity, we consider only the special case of a magnetic field along the direction of the relative superflow $\vec{v}_{sn} = \vec{v}_s - \vec{v}_n$, with $\vec{H} = H\hat{z}$ and $\vec{v}_{sn} = v_0\hat{z}$. To characterize the order parameter, we use the Euler angles α, β, and γ (see Fig. 1) for the orientation of the right triad $\hat{l}$, $\hat{m}$, $\hat{n}$ and the usual polar and azimuthal angles θ and ϕ for the orientation of $\hat{d}$

$$\hat{l} = z\cos\beta + \sin\beta(\hat{x}\cos\alpha + \hat{y}\sin\alpha) \ , \tag{14}$$

$$\hat{d} = \hat{z}\cos\theta + \sin\theta(\hat{x}\cos\phi + \hat{y}\sin\phi) \ . \tag{15}$$

Correspondingly, the superfluid velocity becomes

$$\vec{v}_s = -\vec{\nabla}\gamma - \cos\beta\vec{\nabla}\alpha \ . \tag{16a}$$

Previous studies[3,9] indicate that the instability associated with the helical texture occurs for small-amplitude perturbations with the wave number $\vec{k}$ along $\vec{z}$, and we therefore assume that the order parameter varies spatially only in the z direction. Direct substitution of Eqs. (14) and (15) into Eqs. (16a) and (8) yields

$$v_{sz} = -\gamma' - \alpha'\cos\beta \ , \tag{16b}$$

and

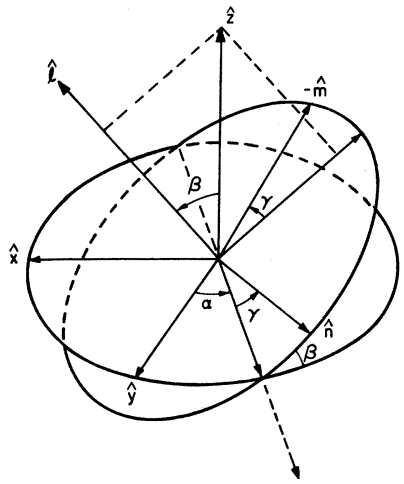

FIG. 1. The Euler angles α, β, and γ that describe the orbital part of the superfluid order parameter.

$$f = \tfrac{1}{2}(\rho_s - \rho_0\cos^2\beta)(-\gamma' - \alpha'\cos\beta - v_n)^2 + C_0\sin^2\beta\cos\beta(-\gamma' - \alpha'\cos\beta - v_n)\alpha'$$
$$+ \tfrac{1}{2}(K_s\sin^2\beta + K_b\cos^2\beta)\beta'^2 + \tfrac{1}{2}(K_t\sin^2\beta + K_b\cos^2\beta)\sin^2\beta\alpha'^2 + \tfrac{1}{2}(K_2\sin^2\beta + K_1\cos^2\beta)(\theta'^2 + \sin^2\theta\phi'^2)$$
$$- \tfrac{1}{2}[\cos\theta\cos\beta + \sin\theta\sin\beta\cos(\alpha - \phi)]^2 + \tfrac{1}{2}H^2\cos^2\theta - \tfrac{1}{2}\rho v_n^2 \ , \tag{17}$$

where the primes denote differentiation with respect to z. The corresponding dynamical equations (9)–(11) become

$$\mu\sin^2\beta(\dot{\alpha} + v_n\alpha') = \left(\frac{\partial f}{\partial \alpha'}\right)' - \frac{\partial f}{\partial \alpha} \ , \tag{18}$$

$$\mu(\dot{\beta} + v_n\beta') = \left(\frac{\partial f}{\partial \beta'}\right)' - \frac{\partial f}{\partial \beta} \ , \tag{19}$$

$$0 = \left(\frac{\partial f}{\partial \gamma'}\right)' - \frac{\partial f}{\partial \gamma} \ , \tag{20}$$

$$0 = \left(\frac{\partial f}{\partial \phi'}\right)' - \frac{\partial f}{\partial \phi} \ , \tag{21}$$

$$0 = \left(\frac{\partial f}{\partial \theta'}\right)' - \frac{\partial f}{\partial \theta} \ , \tag{22}$$

where dots denote differentiation with respect to time and where the partial derivatives are taken holding fixed the other angles and their derivatives.

Inspection of Eq. (17) shows that the free-energy density is now independent of γ. Thus Eq. (20) can be integrated to give [see Eqs. (5), (12), and (13)]

$$-\frac{\partial f}{\partial \gamma'} = j_z^0 \ , \tag{23}$$

where j_z^0 is a spatial constant. This relation serves to eliminate the dynamical variable γ entirely from the problem through a Legendre transformation to a "Routhian" free-energy density[4,24]

$$\tilde{f} = f - \gamma'\frac{\partial f}{\partial \gamma'} = f + \gamma' j_z^0 \ . \tag{24}$$

By construction, $\tilde{f}$ is a function of the angles α, β, θ, ϕ, and the spatial constant j_z^0. It is not difficult to rewrite the dynamical equations in terms of $\tilde{f}$; they are identical with Eqs. (18), (19), (21), and (22) if f is replaced by $\tilde{f}$ and the partial derivatives are taken holding j_z^0 fixed instead of γ'. Equation (20) then holds automatically, reducing the number of dynamical equations from five to four. The choice for f or $\tilde{f}$ in the dynamical equations is merely a matter of con-

venience, for either will work with proper attention to the fixed variables. Under some circumstances, however, one of the two formulations may simplify the calculations.

In addition to the dynamical equations, the order parameter has rather special constraints arising from the "super" character of the fluid. These constraints depend crucially on the mechanism that induces the relative superfluid velocity v_{sn}. An experiment that establishes a persistent current in a toroidal container[1] requires "topological" conditions that ensure the single valuedness of the order parameter. To model this situation, we assume that the normal-fluid velocity vanishes in the frame moving with the walls of the torus. In our one-dimensional model, periodic boundary conditions over a length L in the z direction then simulate the multiply connected geometry. These periodic boundary conditions require that the angles α, γ, and ϕ have well-defined integral winding numbers n_α, n_γ, and n_ϕ

$$\left.\begin{aligned}\alpha(z+L)&=\alpha(z)+2\pi n_\alpha \\ \gamma(z+L)&=\gamma(z)+2\pi n_\gamma\end{aligned}\right\}\ \cos\beta\neq\pm1 \qquad (25a),\ (25b)$$

$$\phi(z+L)=\phi(z)+2\pi n_\phi\ \cos\theta\neq\pm1 \qquad (26)$$

when $\cos\beta\neq\pm1$ and $\cos\theta\neq\pm1$. Thus, in general, the periodic boundary conditions quantize these winding numbers. Moreover, any change in these quantized winding numbers requires that the magnitude of the order parameter vanish over a significant fraction of the fluid; hence transitions between states of different quantized winding numbers encounter large free-energy barriers, which helps account for the assumed metastability of persistent currents in ^{3}He-A.[12] One unique and important feature, however, is that n_ϕ is no longer defined when $\cos\theta=\pm1$, and that n_α and n_γ are not separately quantized when $\cos\beta=\pm1$. Instead, when $\cos\beta=\pm1$, the angles α and γ both generate rotations of $\hat{m}$ and $\hat{n}$ about $\hat{l}$. The single-valuedness condition then requires only that $n_\alpha\pm n_\gamma$ be quantized. Under certain conditions (discussed in Sec. V), these topological properties can allow the winding numbers (and hence the persistent currents) in a toroidal geometry to change without the system having to cross large free-energy barriers.[1]

An alternative procedure for establishing a relative superflow is to impose a heat flow across the sample. In this case, we imagine the system to be confined between two parallel slabs separated by a distance L. In a superfluid, heat flow can exist even in the absence of a temperature gradient. The heat flow $T\rho s v_n\hat{z}$ is carried by the normal fluid, where ρs is the entropy density. In order to conserve mass at the walls, an opposing supercurrent flows across the sample. Equations (13) and (20) imply that $j_z^0=j_{sz}+j_{nz}-v_{nz}$ must be a spatial constant. At the walls, the total z component of the current $j_{sz}+j_{nz}$ vanishes,[25] so that, for heat flow

$$j_z^0=-\rho v_n \ . \qquad (27)$$

As a result, j_z^0 in a thermal counterflow is fixed externally, independent of the textural configuration within the sample. This differs significantly from a persistent current in a torus, where j_z^0 also remains a spatial constant, but whose magnitude depends on the texture.

The preceding discussion shows that the principal difference between persistent current in a torus and heat flow is the nature of the constraints. In a toroidal container, the single valuedness imposes topological conditions on the relative superflow; in heat flow, the current j_z^0 is fixed externally, and the condition of zero mass flow through the walls requires a relative superflow. It is clear from these constraints that the free-energy density f, which has the angles α, β, γ, θ, and ϕ as its natural variables, is the appropriate function for persistent currents in a torus. Similarly, a one-dimensional heat flow is most simply analyzed in terms of the "Routhian" free-energy density $\tilde{f}$, which has α, β, j_z^0, θ, and ϕ as its natural variables.

III. TIME-INDEPENDENT TEXTURES

In the absence of an applied magnetic field or imposed superflow, the equilibrium texture has $\hat{l}$ and $\hat{d}$ parallel and spatially uniform, but in an arbitrary direction. Application of a relative flow or a magnetic field then orients $\hat{l}$ and $\hat{d}$ to minimize the free energy. It is not difficult to show that the dynamical equations have static uniform solutions for all values of the magnetic field $H\hat{z}$ and relative superflow $v_0\hat{z}$, although $\hat{l}$ and $\hat{d}$ are not, in general parallel. These uniform textures can only be realized physically if they are stable against small-amplitude fluctuations. Appendix A outlines the linear-stability analysis of these uniform textures, with the results indicated in Fig. 2.

The most notable conclusion is that dynamically stable uniform textures occur only for values of H and v_0 within the regions labeled I and II of Fig. 2. In region I, where the flow predominates and the field is a small perturbation, the texture with $\hat{l}=\hat{d}=\hat{z}$ is stable. Determining the entire bounding curve requires numerical analysis,[5,9] but the stability for dipole-locked deformations ($\hat{d}\parallel\hat{l}$) at small v_0 and H gives the limiting curve

$$H_0=[\rho_0-(C_0+\tfrac{1}{2})^2(K_b^L)^{-1}]^{1/2}v_0 \qquad (28a)$$

near the origin of region I, where

$$K_b^L=K_b+K_1 \qquad (28b)$$

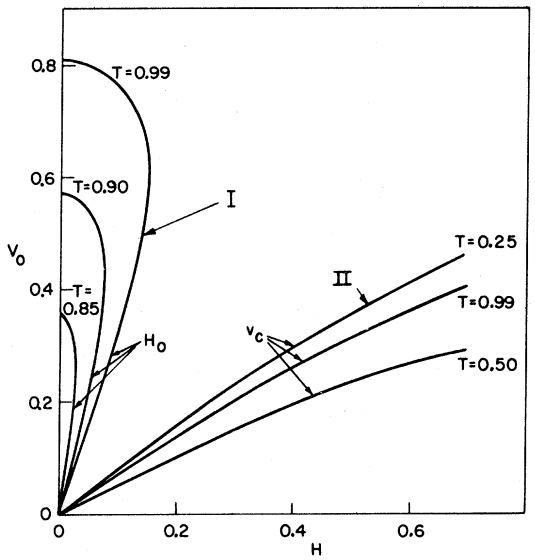

FIG. 2. Phase diagram for textures of ^{3}He-A in a magnetic field $H\hat{z}$ and a parallel relative superflow $v_0\hat{z}$. Uniform textures with $\hat{l}=\hat{d}=\hat{z}$ are stable in region I; uniform textures with $\hat{l}=\hat{d}\perp\hat{z}$ are stable in region II; uniform textures are unstable elsewhere in the Hv_0 plane.

is the dipole-locked elastic constant. In region II, the magnetic field predominates, and the stable texture has $\hat{z}\perp\hat{d}=\hat{l}=\hat{x}$ (say), with the analytic boundary curve

$$v_c=(\rho_0\rho_s)^{-1/2}H(1+H^2)^{-1/2}\ . \tag{29}$$

Although the analysis of these two boundary curves is formally similar, the detailed instability has markedly different forms. In region I, the textures become unstable for plane-wave fluctuations along the z axis of *finite* wave number k_c [see Eq. (A12)]. In region II, however, the texture in a finite quantization volume L^3 first undergoes a uniform small-angle rotation ($k=0$) of order L^*/L in the xz plane, which then becomes unstable[26] with respect to long-wavelength fluctuations with $\hat{k}$ slightly different from $\hat{l}$. Furthermore, the two regions I and II have a very different temperature dependence. As the temperature decreases, region I shrinks monotonically, eventually disappearing when $T\approx 0.82T_c$. In contrast, region II shrinks slightly with decreasing temperature until $T\approx 0.48T_c$ and then increases rapidly as T is lowered below that value. This latter behavior arises largely from the temperature dependence of the anisotropy parameter ρ_0. Some of these predicted temperature effects are probably unobservable because the A-B transition already occurs at $\approx 0.75T_c$ in low fields.

It is striking that region I terminates at a maximum relative superflow, beyond which the texture $\hat{l}=\hat{d}=\hat{z}$ is unstable, even in the absence of an applied field.[9] This feature, which would not occur for a dipole-locked system, reflects the competition between the bending energy and the dipole energy on $\hat{d}$. The finite wave number k_c of the instability at the boundary of region I increases monotonically and nearly linearly with v_0. For large v_0, dipole locking in the deformed phase would require large elastic energy, and it eventually becomes preferable to separate $\hat{d}$ and $\hat{l}$, thus reducing the total bending energy. In effect, allowing $\hat{d}$ full freedom reduces the stiffness of the uniform texture and enhances the instability of the uniform texture with $\hat{d}=\hat{l}=\hat{z}$ to finite-wavelength perturbations.

It is notable that the two regions I and II of stability have only the point $H=v_0=0$ in common. As a result, it is impossible to move continuously from one stable uniform texture to the other without first reducing both the field and the relative superflow to zero. This suggests that the final textural configuration need not be single valued in H and v_0; instead, it depends on the detailed history of the system's preparation. As a particular example, the present study considers the evolution of textures under increasing magnetic stress at fixed initial relative superflow. Specifically, imagine the sample initially prepared with $\vec{v}_{sn}=v_0\hat{z}$; then slowly apply a magnetic field parallel to the superflow. This procedure ensures that the initial texture is a uniform state with $\hat{l}=\hat{d}=\hat{z}$ (region I of Fig. 2). Had the magnetic field been applied before establishing the relative superflow, the initial texture would have been in region II, and the evolution of the system would be very different.

The unusual interest in the instability of the state with $\hat{l}=\hat{d}=\hat{z}$ arises from the finite critical wave number k_c, which suggests that the system evolves into a spatially periodic structure.[1,2] Indeed, the instability of this uniform state has been proved to signal the onset of a Landau displacive transition[3,4] to a helical texture with a spatial period $2\pi/k_c$ (Fig. 3). The polar angles of $\hat{l}$ and $\hat{d}$ acquire constant nonzero values β_0 and θ_0, and the corresponding azimuthal angles α and ϕ increase linearly in the z direction. The helix is carried along with the normal-fluid velocity, giving α and ϕ a trivial nondissipative time dependence. Thus solutions to the dynamical equations have the form

$$\alpha=-u(z-v_nt)\ , \tag{30}$$

$$\beta=\beta_0\ , \tag{31}$$

$$\gamma=-sz+F(t)\ , \tag{32}$$

$$\theta=\theta_0\ , \tag{33}$$

$$\phi=-u(z-v_nt)\ , \tag{34}$$

where β_0, θ_0, u, and s are spatial constants, and $F(t)$ depends only on t.

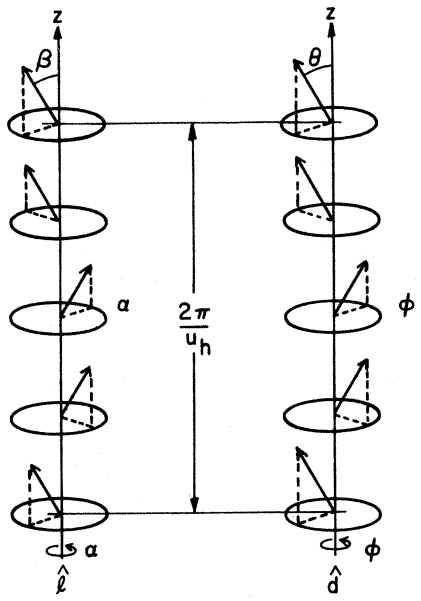

FIG. 3. Helical texture with pitch u_h, showing the polar and azimuthal angles of $\hat{l}(\beta,\alpha)$ and $\hat{d}(\theta,\phi)$.

The appropriate values of s and u follow from the constraints imposed by the experimental situation. In the toroidal geometry, the uniform texture with $\hat{l}=\hat{d}=\hat{z}$ and $\beta_0=\theta_0=0$ fixes only the winding number of the sum $\alpha+\gamma$, which requires that $u+s$ be quantized in units of $2\pi/L$. If the original relative superflow is $v_0=v_{sz}-v_n$, this condition may be written as [see Eq. (16b)] (for a torus)

$$s-v_n=v_0-u \ . \tag{35}$$

Once the helix appears with nonzero β_0 and θ_0, however, the winding numbers of α and γ become separately quantized.[11,12] This distortion fixes the "pitch" u of the helix. In addition, s retains the value from Eq. (35), independent of β_0, so that the relative superflow $v_{sz}-v_n$ becomes an explicit function of β_0 and u (for a torus)

$$v_{sz}-v_n=v_0+u\,(\cos\beta_0-1) \ . \tag{36}$$

On the other hand, heat flow imposes the condition that the total current vanish for all β_0, which requires s to be an explicit function of β_0. Use of Eqs. (16b), (23), and (27) yields the expression (for heat flow)

$$j_z^0=(\rho_s-\rho_0\cos^2\beta_0)(s+u\cos\beta_0-v_n) - C_0u\sin^2\beta_0\cos\beta_0=-\rho v_n \ , \tag{37a}$$

and any alteration of the texture must keep this quantity fixed. Equivalently, we may rewrite this relation as (for heat flow)

$$s-v_n=(v_0+C_0u\sin^2\beta_0\cos\beta_0)\times(1+\rho_0\sin^2\beta_0)^{-1}-u\cos\beta_0 \ , \tag{37b}$$

where $v_0=-\rho v_n$ is the original relative superflow in the uniform state. Note that s is not quantized in this latter situation.

For both the torus and the heat flow, the pitch u of the helix when the system first distorts to have $\beta_0\neq 0$ is just the critical wave number k_c from Eq. (A12). As β_0 increases with increasing H, this pitch remains constant, because any small change in u would imply a large deformation in the order parameter, with $\hat{l}$ changing direction over the whole sample. In a torus, the quantization conditions specifically maintain u when $\beta_0\neq 0$; even in heat flow, however, changing the pitch of the helix in any geometry that lacks perfect axial symmetry would encounter large free-energy barriers.

If we substitute Eqs. (30)–(34) into the free-energy density and the dynamical equations (19)–(21), we find that β_0 and θ_0 must satisfy the following pair of coupled transcendental equations

$$\sin2(\theta_0-\beta_0)=\sin2\beta_0\{\rho_0(\zeta+u\cos\beta_0)^2+u^2[K_b+2(K_t-K_b)\sin^2\beta_0+(K_2-K_1)\sin^2\theta_0]\} - 2\sin\beta_0\{C_0u(\zeta+u\cos\beta_0)(2-3\sin^2\beta_0)+u[(1+\rho_0\sin^2\beta_0)(\zeta+u\cos\beta_0)-C_0u\sin^2\beta_0\cos\beta_0]\} \ , \tag{38}$$

$$\sin2(\theta_0-\beta_0)=[H^2-u^2(K_2\sin^2\beta_0+K_1\cos^2\beta_0)]\sin2\theta_0 \ , \tag{39}$$

where the parameter ζ denotes $s-v_n$ and is defined differently in the two situations [see Eqs. (35) and (37)]

$$\zeta\equiv s-v_n=\begin{cases} v_0-u \ \text{(torus)} & \text{(40a)} \\ (v_0+C_0u\sin^2\beta_0\cos\beta_0)(1+\rho_0\sin^2\beta_0)^{-1}-u\cos\beta_0 \ \text{(heat flow)} \ . & \text{(40b)} \end{cases}$$

Within region I of Fig. 2, the values $\beta_0 = \theta_0 = 0$ are the only solutions to Eqs. (38) and (39). As the magnetic field strength H is increased with v_0 fixed, the transcendental equations first have nonzero solutions when the system reaches the bounding curve; we denote the corresponding critical magnetic field by H_0, which depends on v_0. The instability of the uniform state signals the onset of a small-angle helical texture, with the pitch u_h determined as the root of the equation [compare Eq. (A12b)]

$$[K_b + K_1(1 - H_0^2 + K_1 u_h^2)^{-2}]u_h = (C_0 + \tfrac{1}{2})v_0 \ . \quad (41)$$

In the dipole-locked limit, v_0 and H are both small; an elementary calculation gives the specific value

$$u_h = (C_0 + \tfrac{1}{2})v_0/K_b^L \ , \quad (42a)$$

which becomes

$$u_h \approx 0.6 v_0 \quad (42b)$$

near T_c. More generally, numerical analysis for the weak-coupling Ginzburg-Landau values ($\rho_0 = C_0 = \frac{1}{2}\rho_s = K_1 = \frac{2}{3}K_b = 1$) shows that u_h/v_0 increases from 0.6 for small v_0 to ≈ 0.74 at the maximum value $v_0 \approx 0.826$. Thus u_h increases nearly linearly with v_0 throughout the allowed range.

It is interesting to note that the initial value of u_h (and hence the initial form of the helical texture) is independent of how the superflow is established, because [see Eq. (40)] $\zeta(\text{torus}) = \zeta(\text{heat flow})$ when β_0 vanishes. Once $\beta_0 \neq 0$, however, the particular experimental arrangement becomes important. Since the pitch of the helix is fixed by the conditions when the texture first deviates from the uniform state, it is essential to specify the details of any experimental procedure. Here we concentrate on textures that evolve as H is increased past H_0 at constant values of the other external variables (such as the temperature T and v_n). This choice implies a horizontal trajectory in the Hv_0 plane of Fig. 2. Many other possibilities exist, and each, in general, requires a separate analysis; a few are mentioned briefly in Sec. VI.

Once the helix appears, it becomes important to investigate its dynamical stability; here we consider only longitudinal variations $\propto e^{ikz}$, since these are thought to be the most critical.[27] First, the equilibrium parameters β_0 and θ_0 of the helical state are determined from Eqs. (38) and (39), assuming that the system evolves from the uniform state with its pitch u_h fixed as the magnetic field increases past H_0. Next, the texture is assumed to undergo small variations about this equilibrium [compare Eqs. (30)–(34)] with $\alpha(z,t) = -u_h(z - v_n t) + \delta\alpha(z,t)$, $\beta(z,t) = \beta_0 + \delta\beta(z,t)$, and corresponding small changes in γ, θ, and ϕ. Finally, the small variations are expanded in Fourier series, for example,

$$\delta\alpha(z,t) = \sum_k \exp(ikz + \sigma t)\delta\alpha_k \ , \quad (43)$$

where $k = 2\pi n/L$; $n = 0, \pm 1, \pm 2, \ldots$; $\delta\alpha_k^* = \delta\alpha_{-k}$, and $|\sigma^{-1}|$ is the characteristic relaxation time of the deformed helix back to its equilibrium configuration. The linearized dynamical equations (18)–(22) for the small variations lead to a determinantal equation for σ as a function of k.[28] The helix is stable only if σ is negative for all values of k. Determining this region of stability is analogous to that for the uniform state (Appendix A), except that it now becomes crucial to distinguish between heat flow and persistent currents in a torus by imposing the appropriate constraints.

We have evaluated numerically the region of stability for a helix subject to longitudinal perturbations, using the hydrodynamic parameters from Ref. 3. As the magnetic field increases beyond H_0, the equilibrium helix develops an ever-increasing opening angle β_0. At a critical magnetic field H_1, the helical texture ceases to be stable against small fluctuations of long, but not infinite, wavelength [namely, $n = \pm 1$ in Eq. (43)]. For a helix of fixed pitch, it is curious that the helices are unstable only in a finite range of magnetic field $H_1 < H < H_2$, and that helices again become

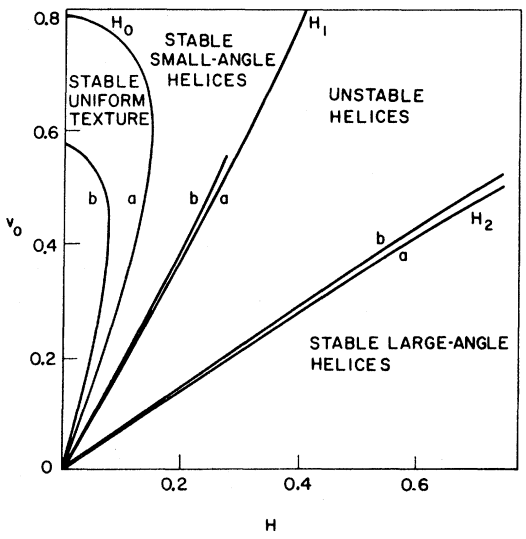

FIG. 4. Stability regions for helices that form in a torus for temperatures $0.99T_c$ (curves a) and $0.90T_c$ (curves b). The helices evolve with increasing magnetic field H at fixed initial relative superflow v_0. The curves for heat flow differ only in minor changes in H_1 and H_2.

TABLE I. Critical opening angle and magnetic field when helix becomes unstable.

	Torus				Heat flow			
v_0	β_1	H_1	β_2	H_2	β_1	H_1	β_2	H_2
				$T=0.99T_c$				
0.1	0.623	0.053	1.84	0.139	0.602	0.052	1.85	0.161
0.3	0.607	0.160	1.85	0.423	0.591	0.157	1.88	0.504
0.5	0.569	0.262	1.88	0.733	0.565	0.261	1.94	0.956
0.7	0.510	0.355			0.531	0.364		
				$T=0.90T_c$				
0.1	0.648	0.050	1.84	0.135	0.643	0.050	1.86	0.163
0.3	0.629	0.150	1.85	0.409	0.633	0.151	1.88	0.514
0.5	0.586	0.247	1.87	0.703	0.610	0.253	1.95	0.985

stable with respect to longitudinal perturbations for $H > H_2$.[29] We denote the opening angles at the two points of instability by β_1 and β_2, respectively. Figure 4 shows the regions of stable helices in a torus for two different temperatures; the situation for heat flow differs only slightly. Table I lists the critical magnetic field and opening angle for $\hat{l}$ at several points along both stability lines. Notice that $\beta_1 \approx 0.6$ ($\approx 35°$) almost independent of temperature and the source of the imposed superflow, and that β_2 exceeds $\frac{1}{2}\pi$.

The helices that are stable in the range $H_0 < H < H_1$ have small opening angles, while those stable for $H > H_2$ have large angles. It is not obvious that these large-angle helices are accessible in an experiment that increases the magnetic field at fixed v_n, because linear stability theory cannot determine the subsequent evolution of the texture beyond the threshold at H_1. The next two sections investigate the nature of the instability at H_1 and suggest a qualitative picture that may provide some insight into the ultimate evolution of the textures.

IV. NONLINEAR STABILITY

The preceding discussion shows that the uniform texture $\hat{l} = \hat{d} = \hat{z}$ in a relative superflow v_0 becomes dynamically unstable at a critical field H_0, signaling the onset of a helical deformation with a specific pitch u_h. This helical texture in turn becomes unstable at a higher critical magnetic field H_1, and it is natural to ask whether this second instability again signals the onset of a new static distortion. To analyze this question, we consider the time evolution of the first unstable mode, including the leading nonlinear contribution. For the onset of the helical deformation at H_0, these nonlinear terms limit the growth,[3,4] leading to a normal bifurcation[16] with the characteristic Landau behavior $\beta_0 \propto (H - H_0)^{1/2}$ just beyond threshold. In contrast, the nonlinear terms in the transition at H_1 will now be shown to enhance the growth, leading to an inverted bifurcation and a catastrophic instability. For simplicity, we consider only the dipole-locked limit.

In the case of one-dimensional motion, the dipole-locked free-energy density (17) becomes

$$f = \tfrac{1}{2}(1+\rho_0 \sin^2\beta)(\alpha' \cos\beta + \gamma' + v_n)^2 - C_0 \alpha' \sin^2\beta \cos\beta(\alpha' \cos\beta + \gamma' + v_n)$$
$$+ \tfrac{1}{2}\sin^2\beta(K_b^L \cos^2\beta + K_t^L \sin^2\beta)\alpha'^2 + \tfrac{1}{2}(K_b^L \cos^2\beta + K_s^L \sin^2\beta)\beta'^2 + \tfrac{1}{2}H^2 \cos^2\beta \ , \tag{44}$$

where we have set $\theta = \beta$, $\phi = \alpha$, dropped the additional constant terms $-\frac{1}{2}(1+\rho v_n^2)$, and introduced the dipole-locked parameters [compare Eq. (28b)]

$$K_b^L = K_b + K_1, \quad K_s^L = K_s + K_2, \quad K_t^L = K_t + K_2 \ . \tag{45}$$

In general, the current

$$j_z^0 = -\frac{\partial f}{\partial \gamma'} = -(1+\rho_0 \sin^2\beta)(\alpha' \cos\beta + \gamma' + v_n) + C_0 \alpha' \sin^2\beta \cos\beta \tag{46}$$

is a spatial constant of the motion that depends of the particular experiment in question. For a thermal counterflow, the heat flux itself determines j_z^0, independent of the helical texture at the onset of instability. In a torus, however, this constant depends on the specific parameters of the helix [see Eqs. (30)–(32) and (35)]:

$$j_z^0 = (1+\rho_0 \sin^2\beta_0)[v_0 + u_n(\cos\beta_0 - 1)] - C_0 u_h \sin^2\beta_0 \cos\beta_0 \ . \tag{47}$$

In either case, the subsequent evolution of the variables α, β, and γ for $H > H_1$ must preserve this constant. Thus the problem can be simplified considerably by introducing the Routhian free-energy density [see Eq. (24)]

$$\tilde{f} = f - \gamma' \frac{\partial f}{\partial \gamma'} = \tfrac{1}{2}\sin^2\beta \left[K_b^L \cos^2\beta + K_t^L \sin^2\beta - \frac{C_0^2 \cos^2\beta \sin^2\beta}{1+\rho_0 \sin^2\beta} \right] \alpha'^2 - j_z^0 \cos\beta \frac{1+(\rho_0 - C_0)\sin^2\beta}{1+\rho_0 \sin^2\beta} \alpha'$$
$$- \tfrac{1}{2} \frac{(j_z^0)^2}{1+\rho_0 \sin^2\beta} - j_z^0 v_n + \tfrac{1}{2}(K_b^L \cos^2\beta + K_s^L \sin^2\beta)\beta'^2 + \tfrac{1}{2} H^2 \cos^2\beta \ , \tag{48}$$

which now depends only on the two dynamical variables $\alpha(z,t)$ and $\beta(z,t)$. The corresponding dynamical equations become

$$\mu \sin^2\beta (\dot{\alpha} + v_n \alpha') = \left(\frac{\partial \tilde{f}}{\partial \alpha'} \right)' \ , \tag{49a}$$

$$\mu (\dot{\beta} + v_n \beta') = \left(\frac{\partial \tilde{f}}{\partial \beta'} \right)' - \frac{\partial \tilde{f}}{\partial \beta} \ . \tag{49b}$$

The steady helix is characterized by the azimuthal angle $\alpha_0 = -u_h(z - v_n t)$ and a constant polar angle β_0, and we therefore write

$$\alpha = \alpha_0 + \delta\alpha, \quad \beta = \beta_0 + \delta\beta \ . \tag{50}$$

Substitution into Eqs. (48) and (49) yields the exact relations

$$\mu \sin^2\beta (\dot{\delta\alpha} + v_n \delta\alpha') = \frac{\partial^2 \tilde{f}}{\partial \alpha'^2} \delta\alpha'' + \frac{\partial^2 \tilde{f}}{\partial \alpha' \partial \beta} \delta\beta' \ , \tag{51a}$$

$$\mu (\dot{\delta\beta} + v_n \delta\beta') = \left(\frac{\partial^2 \tilde{f}}{\partial \beta'^2} \delta\beta' \right)' - \frac{\partial \tilde{f}}{\partial \beta} \ , \tag{51b}$$

where the partial derivatives themselves still depend on the full dynamical variables. It is now straightforward to expand the coefficients about the steady helical texture. Introducing the abbreviations $x \equiv \delta\alpha$ and $y \sin\beta_0 \equiv \delta\beta$, we find the following approximate equations

$$\mu (\dot{x} + v_n x')(1 + 2y\cos\beta_0 + \cdots)$$
$$= a x'' + b y' + e(x''y + x'y') + f y' y + \cdots \ , \tag{52a}$$

$$\mu (\dot{y} + v_n y') = -b x' + d y'' - c y - \tfrac{1}{2} e x'^2 - f x' y - \tfrac{1}{2} g y^2$$
$$+ h(y''y + \tfrac{1}{2} y'^2) + \cdots \ . \tag{52b}$$

Here the terms omitted are of third order in the small quantities and can be shown not to contribute in leading order since the instability occurs at long wavelengths. The constant coefficients in Eq. (52) denote various partial derivatives of $\tilde{f}$ evaluated in the equilibrium helical configuration

$$a = \frac{1}{\sin^2\beta_0} \left(\frac{\partial^2 \tilde{f}}{\partial \alpha'^2} \right)_0 \ , \quad b = \frac{1}{\sin\beta_0} \left(\frac{\partial^2 \tilde{f}}{\partial \alpha' \partial \beta} \right)_0 \ ,$$
$$c = \left(\frac{\partial^2 \tilde{f}}{\partial \beta^2} \right)_0 \ , \quad d = \left(\frac{\partial^2 \tilde{f}}{\partial \beta'^2} \right)_0 \ ,$$
$$e = \frac{1}{\sin\beta_0} \left(\frac{\partial^3 \tilde{f}}{\partial \alpha'^2 \partial \beta} \right)_0 \ , \quad f = \left(\frac{\partial^3 \tilde{f}}{\partial \alpha' \partial \beta^2} \right)_0 \ , \tag{53}$$
$$g = \sin\beta_0 \left(\frac{\partial^3 \tilde{f}}{\partial \beta^3} \right)_0 \ , \quad h = \sin\beta_0 \left(\frac{\partial^3 \tilde{f}}{\partial \beta'^2 \partial \beta} \right)_0 \ .$$

A general deformation of the helix may be expanded in plane waves of the form

$$x(z,t) = \sum_m e^{imk_0 z} x_m(t) \ , \quad y(z,t) = \sum_m e^{imk_0 z} y_m(t) \ , \tag{54}$$

where $k_0 = 2\pi/L$, and the Fourier coefficients satisfy the relations

$$x_{-m}(t) = x_m(t)^*, \quad y_{-m}(t) = y_m(t)^* \ . \tag{55}$$

Before studying the nonlinear evolution, it is helpful to consider the linearized equations for the mth mode

$$\mu (\dot{x}_m + imk_0 v_n x_m) \approx -m^2 k_0^2 a x_m + imk_0 b y_m \ , \tag{56a}$$

$$\mu (\dot{y}_m + imk_0 v_n y_m) \approx -imk_0 b x_m - (c + m^2 k_0^2 d) y_m \ . \tag{56b}$$

These have solutions of the form $e^{\sigma t}$ [compare Eq. (43)] and a simple calculation gives the allowed values

$$\mu(\sigma_m^{(\pm)}+imk_0v_n)=-\tfrac{1}{2}[c+m^2k_0^2(a+d)]\pm\{\tfrac{1}{4}[c+m^2k_0^2(a+d)]^2+m^2k_0^2(b^2-ac-m^2k_0^2ad)\}^{1/2} \quad . \tag{57}$$

It follows by inspection that a and d are positive; furthermore, Figs. 5(c) and 5(e) show that c is also positive (if c were negative, the helix would be unstable with respect to a uniform increase in the polar angle β_0). Thus the instability first occurs for $m=1$, when $\mathrm{Re}\sigma_1^{(+)}$ changes from negative to positive, at the field H_1 determined by the condition

$$b^2-ac=k_0^2ad \quad . \tag{58}$$

Since k_0 is small for a macroscopic system, this long-wavelength instability appears approximately when the determinant of second partial derivatives $ac-b^2$ first vanishes.[4]

The corresponding normal modes are linear combinations of x_m and y_m:

$$\xi_m=p_mx_m+iq_my_m, \quad \eta_m=iq_mx_m+p_my_m \quad , \tag{59}$$

with the growth constants $\sigma_m^{(+)}$ and $\sigma_m^{(-)}$, respectively. Here, the coefficients p_m and q_m are given by

$$p_m=N_m\{\tfrac{1}{2}[c+m^2k_0^2(d-a)]+S_m\}, \quad q_m=N_mmk_0b \quad , \tag{60}$$

and

$$N_m^{-2}=2S_m\{\tfrac{1}{2}[c+m^2k_0^2(d-a)]+S_m\} \quad , \tag{61a}$$

$$S_m^2=\tfrac{1}{4}[c+m^2k_0^2(d-a)]^2+m^2k_0^2b^2 \quad . \tag{61b}$$

Note that $p_m^2+q_m^2=1$, so that Eq. (59) is readily inverted to give

$$x_m=p_m\xi_m-iq_m\eta_m, \quad y_m=-iq_m\xi_m+p_m\eta_m \quad . \tag{62}$$

In addition, p_m is of order 1 and q_m is of order $k_0a/b\approx(Lv_0)^{-1}\approx L^*/L\ll 1$, implying that the dominant motion in the unstable normal mode is torsional.

We now return to the exact nonlinear dynamical equations (52) and construct the linear combinations appropriate for the normal modes ξ_m. Substituting the Fourier expansions (54), we find

$$\mu(\dot{\xi}_m+imk_0\xi_m)=\mu\sigma_m^{(+)}\xi_m+\sum_n\{-p_m\mu(\dot{x}_n+ink_0x_n)2\cos\beta_0y_{m-n}-p_memnk_0^2x_ny_{m-n}+ip_mfnk_0y_ny_{m-n}$$
$$+\tfrac{1}{2}iq_men(m-n)k_0^2x_nx_{m-n}+q_mfnk_0x_ny_{m-n}-\tfrac{1}{2}iq_m[g+hn(m+n)k_0^2]y_ny_{m-n}\}$$
$$+\cdots \quad , \tag{63}$$

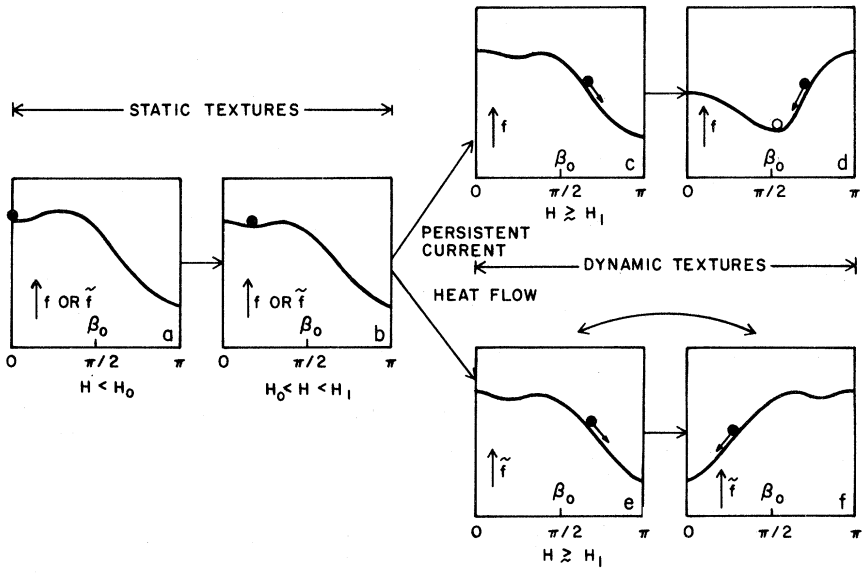

FIG. 5. Evolution of the free-energy density of helical textures with increasing magnetic stress. See text (Sec. V) for detailed description.

with a similar equation for η_m. In the regime

$$k_0^2 ad \leq b^2 - ac \leq 4k_0^2 ad \ , \tag{64}$$

just above threshold, only the lowest normal mode ξ_1 grows with time in the linearized approximation. Thus we assume that $\xi_1(t)$ has the form

$$\xi_1(t) = A(t) \exp(-ik_0 v_n t) \ , \tag{65}$$

where $A(t)$ is a small time-dependent amplitude.

Equation (62) shows that $x_1(t)$ and $y_1(t)$ are each of order A, since the dynamical equation for η_1 indicates that it is of higher order (A^3). Thus, to leading order, we may write

$$\begin{aligned} x_1 &\approx p_1 \xi_1 = p_1 A \exp(-ik_0 v_n t) \ , \\ y_1 &\approx -iq_1 \xi_1 = -iq_1 A \exp(-ik_0 v_n t) \ . \end{aligned} \tag{66}$$

The dynamical equation for A follows from Eq. (63) for $m = 1$:

$$\begin{aligned} &\mu(\dot{A} - \sigma_1^{(+)} A) \exp(-ik_0 v_n t) \\ &\quad = -2\mu \cos\beta_0 p_1 [(\dot{x}_{-1} - ik_0 v_n x_{-1}) y_2 + \dot{x}_0 y_1 + (\dot{x}_1 + ik_0 v_n x_1) y_0 + (\dot{x}_2 + 2ik_0 v_n x_2) y_{-1} + \cdots] \\ &\qquad - p_1 e k_0^2 (-x_{-1} y_2 + x_1 y_0 + 2x_2 y_{-1} + \cdots) + ip_1 f k_0 (-y_{-1} y_2 + y_1 y_0 + 2y_2 y_{-1} + \cdots) \\ &\qquad + \tfrac{1}{2} iq_1 e k_0^2 (-2x_{-1} x_2 - 2x_2 x_{-1} + \cdots) + q_1 f k_0 (-x_{-1} y_2 + x_1 y_0 + 2x_2 y_{-1} + \cdots) \\ &\qquad - \tfrac{1}{2} iq_1 [g(y_{-1} y_2 + y_0 y_1) + (g + 2hk_0^2) y_1 y_0 + (g + 6hk_0^2) y_2 y_{-1} + \cdots] \ , \end{aligned} \tag{67}$$

so that the nonlinear coupling among the modes introduces higher-order terms in A.

To identify the particular terms of importance, we consider the corresponding equation (63) for ξ_2, retaining only the leading nonlinearities (of order A^2):

$$\begin{aligned} \mu(\dot{\xi}_2 + 2ik_0 v_n \xi_2) &= \mu \sigma_2^{(+)} \xi_2 - 2\mu \cos\beta_0 p_2 (\dot{x}_1 + ik_0 v_n x_1) y_1 - 2p_2 e k_0^2 x_1 y_1 + ip_2 f k_0 y_1^2 \\ &\quad + \tfrac{1}{2} iq_2 e k_0^2 x_1^2 + q_2 f k_0 x_1 y_1 - \tfrac{1}{2} iq_2 (g + 3hk_0^2) y_1^2 + \cdots \ . \end{aligned} \tag{68}$$

Substitution of Eq. (66) on the right-hand side shows that $\xi_2(t)$ has the form

$$\xi_2(t) = \xi_2^{(2)} A^2 \exp(-2ik_0 v_n t) \ , \tag{69}$$

where

$$\begin{aligned} \mu \sigma_2^{(+)} \xi_2^{(2)} = -i [& p_1 (2p_2 q_1 + \tfrac{1}{2} p_1 q_2) e k_0^2 \\ & - q_1 (p_2 q_1 + p_1 q_2) f k_0 \\ & + \tfrac{1}{2} q_2 q_1^2 (g + 3hk_0^2)] \ . \end{aligned} \tag{70}$$

Here terms of order $\dot{A}A$ have been neglected since, by assumption, the initial growth rate of A is small. At threshold, Eqs. (57) and (58) imply that $\mu \sigma_2^{(+)} = -12 k_0^4 da/c$, and use of Eqs. (60) and (61) leads to the relation

$$\xi_2^{(2)} \approx \frac{ib}{12 k_0 da} \left(3e - \frac{3fa}{b} + \frac{ga^2}{b^2} \right) \ , \tag{71}$$

neglecting terms of higher order in $k_0 a/b \ll 1$. Similarly, $\xi_0(t)$ has the form $\xi_0^{(2)} A^2$, but the coefficient $\xi_0^{(2)}$ turns out to vanish to this order. In addition, both $\eta_0(t)$ and $\eta_2(t)$ are also of order A^2, but the corresponding coefficients are smaller than $\xi_2^{(2)}$ in Eq. (71) by a factor of order $(k_0 a/b)^3$. Thus only the single mode ξ_2 contributes to Eq. (67) in the present long-wavelength limit.

It is now straightforward to evaluate the right-hand side of Eq. (67) to leading order in powers of A. Equation (62) and (69) give

$$\begin{aligned} x_2(t) &\approx p_2 \xi_2^{(2)} A^2 \exp(-2ik_0 v_n t) \ , \\ y_2(t) &\approx iq_2 \xi_2^{(2)} A^2 \exp(-2ik_0 v_n t) \ , \end{aligned} \tag{72}$$

and the corresponding x_0 and y_0 are negligible. Use of Eqs. (55) and (71) eventually leads to the desired relation

$$\mu \dot{A} = \mu \sigma_1^{(+)} A + \frac{k_0^2}{6d} \left(3e - \frac{3fa}{b} + \frac{ga^2}{b^2} \right)^2 A^3 \ , \tag{73}$$

neglecting higher-order terms in the small parameter $k_0 a/b$.[30] The most significant feature of this equation is that the A^3 term has a positive-definite coefficient. Below threshold ($\mathrm{Re}\sigma_1^{(+)} < 0$), an infinitesimal initial perturbation $A(0)$ decays exponentially to zero and the cubic term remains negligible. Just above threshold, however, $\mathrm{Re}\sigma_1^{(+)}$ becomes positive and an initial perturbation $A(0)$ grows exponentially until the cubic term becomes appreciable. The solution then changes character and apparently diverges at some finite time. The present approximation cannot analyze this ultimate behavior in detail, but the form of Eq. (73) clearly indicates the onset of a catastrophic instability that is not merely a small deformation to some nearby state. Similar inverted bifur-

cations are found in certain hydrodynamic problems.[16]

The constants in Eq. (53) depend on the particular experiment in question. Weak-coupling values of the dipole-locked hydrodynamic parameters near T_c yield the following critical values for the onset of instability

$$\begin{aligned} &\beta_1 = 0.622, \quad H_1 = 0.538 v_0 \text{ (torus)} , \\ &\beta_1 = 0.599, \quad H_1 = 0.527 v_0 \text{ (heat flow)} , \end{aligned} \tag{74}$$

essentially the same as those in Table I, where dipole locking was not imposed. Correspondingly, numerical evaluation of the various partial derivatives yields the value $3e - 3fa/b + ga^2/b^2 \approx -0.632$ for a torus and ≈ -0.046 for heat flow.[31]

V. TIME-DEPENDENT TEXTURES

The preceding analysis suggests that the instability of the helical texture at H_1 does not produce a small deformation to another more complicated static texture. Rather, the inverted bifurcation probably indicates the onset of time-dependent dissipative textures.

To gain qualitative insight into the character of the instability, it is useful to consider the form of the free energy as a function of the opening angle of the helix. A stationary equilibrium texture corresponds to a local minimum of the free energy appropriate to the experiment in question. The free-energy density f with the natural variables α, β, γ, θ, ϕ is therefore the appropriate function for a persistent current in a torus. In heat flow, the relevant function is $\tilde{f}$, which has α, β, j_z^0, θ, ϕ as its natural variables.

As illustrated in Fig. 5, f and $\tilde{f}$ are similar for $H < H_1$. They both have a local minimum at $\beta_0 = 0$ for $H < H_0$, which represents the uniform state with $\hat{d} = \hat{l} = \hat{z}$ [Fig. 5(a)]. The onset of a helical state at H_0 occurs when the curvature at $\beta_0 = 0$ changes sign [Fig. 5(b)]. The local minimum at $\beta_0 = 0$ now becomes a local maximum, and the system undergoes a typical Landau transition to the new local minimum at $\beta_0 \neq 0$. Once H exceeds H_0 and β_0 is nonzero, the pitch u_h of the helix is fixed by the initial relative superflow. The free-energy density then becomes a function of u_h, and *textures with different values of u_h evolve differently with increasing magnetic field.*

As $H - H_0$ grows from zero, the opening angle of the helix increases continuously. When the helix first becomes dynamically unstable at H_1, the free energy still appears to have a local minimum at $\beta_0 - \beta_1$ [recall $c > 0$ but $ac - b^2 \approx 0$ in Eqs. (53) and (58)]. If the texture were only a function of the constant polar angle β_0, the helix would indeed be stable at H_1, but the additional degrees of freedom associated with nonuniform motion introduce more and different fluctuations. In this general parameter space, the free energy acquires a saddle point that allows the helix to deform spontaneously for $H > H_1$ [Figs. 5(c) and 5(e)].

Once the system has left the local minimum representing a stable helical state, it is likely to evolve into a more complicated configuration. Nevertheless, the form of the free energy for a helical texture provides valuable insight into the subsequent dynamical evolution. Figures 5(c) and 5(e) suggest that the texture then becomes intrinsically time dependent (and dissipative through the Cross-Anderson viscosity). The dynamical equations drive the system toward lower free energy, and the texture thus moves to the reversed configuration with $\beta_0 = \pi$.

As long as the helical textures are stable, the practical difference between a torus and heat flow is negligible (compare Table I). After the helical textures become unstable, however, the opening angle increases toward π, and the difference becomes significant. For example, the instantaneous value of $v_{sz} - v_n$ is increasingly different in the two cases as β_0 grows [see Eqs. (36) and (37)]

$$v_{sz} - v_n = \begin{cases} v_0 - (1 - \cos\beta_0) u_h & \text{(torus)} \\ \dfrac{v_0 + C_0 u_h \sin^2\beta_0 \cos\beta_0}{1 + \rho_0 \sin^2\beta_0} & \text{(heat flow)} . \end{cases} \tag{75}$$

Recall that v_0 is the relative superflow in the original uniform texture, taken to be the same in the two configurations. When the time-dependent texture in the torus has reached $\beta_0 = \pi$, the relative superflow $v_{sz} - v_n$ has the new value $\bar{v}_0$ given by $\bar{v}_0 = v_0 - 2u_h$. The dipole-locked limit near T_c yields the values $u_h = 0.6 v_0$, and $\bar{v}_0 = -0.2 v_0$, and other situations will be qualitatively similar. In particular, we notice that the direction of the relative supercurrent has *reversed,* and its magnitude is markedly reduced. In an external heat flow, on the other hand, when the texture reaches $\beta_0 = \pi$, Eq. (75) shows that the relative superflow is once again v_0, the same as in the original uniform state. Thus the instability of helical textures leads to dramatically different configurations in a torus and in heat flow.

The time-dependent process does not stop at $\beta_0 = \pi$, however, for the texture is now essentially uniform with $\hat{l}$ and $\hat{d}$ along $-\hat{z}$, but in a finite magnetic field $H > H_1$. For persistent flow in a torus, the relative superflow in reduced and reversed, and detailed analysis shows that this new uniform state is once again unstable with respect to the formation of a helical texture. Imagine the system to fluctuate about $\beta_0 = \pi$ in a superposition of different plane-wave states. The maximum growth rate in the dipole-locked regime occurs for a characteristic wave number $\bar{k}_c$, leading to the formation of a helix with pitch $\bar{u}_h = \bar{k}_c = -(C_0 + \frac{1}{2})\bar{v}_0 / K_b^L$. Since the free energy depends on the pitch, the change from u_h to $\bar{u}_h$

alters the form of f qualitatively [compare Figs. 5(a) and 5(d)]. In fact, the new free-energy density has a deep local minimum near $\beta_0 = \frac{1}{2}\pi$ that is stable with respect to small-amplitude longitudinal perturbations. Presumably, the system relaxes to this new minimum, thus providing a mechanism for attaining the stable wide-angle helices shown as the region $H > H_2$ in Fig. 4. In essence, the reduction in the relative superflow from v_0 to $\bar{v}_0$ drops the system along the vertical line $H = H_1(v_0)$ into the region below the curve H_2 in Fig. 4.

In heat flow, the new uniform texture again has $\hat{l} = \hat{d} = -\hat{z}$ and $H > H_1$, but the relative superflow retains its original value v_0. This state is also unstable with respect to small-amplitude fluctuations, with the maximum growth rate now occurring for $\bar{u}_h = -u_h$. Thus the system presumably develops into a helix with equal and opposite winding. The new free-energy density $\tilde{f}(\beta_0)$ in Fig. 5(f) is obtained with the substitution $u_h \rightarrow -u_h$; it is simply the reflection of the original curve in Fig. 5(e) about $\beta_0 = \frac{1}{2}\pi$. The system is now at a local maximum and begins to decrease β_0 from π. The local minimum at β_1 is again unstable because $H > H_1$, and the system therefore evolves by decreasing the polar angle continuously to zero. At $\beta_0 = 0$, the texture has returned to the original uniform configuration, and the process can repeat. Thus the texture in a heat flow oscillates from $\beta_0 = 0$ to $\beta_0 = \pi$, continuously dissipating energy supplied by the heat source.[32] The motion is anharmonic because of the shape of $\tilde{f}(\beta_0)$. Since $\partial\tilde{f}/\partial\beta_0$ vanishes at several points along $\tilde{f}(\beta_0)$, fluctuations or boundary conditions that distort the texture must be invoked to maintain the motion. As a result, the present dynamical equations are insufficient to deduce the period of the motion.

These qualitative considerations have been based solely on helical configurations, whereas the actual textures that appear beyond H_1 are almost certainly more complicated. In addition, the presence of boundaries introduces surface layers. Both of these effects may help explain the intricate periodic motions for heat flow found by Hook and Hall[8] through numerical integration for one-dimensional textures in a finite channel.

VI. DISCUSSION

This work has concentrated on one class of helical textures in superfluid ^{3}He-A. The system is initially prepared with a relative superflow v_0 and then subjected to a parallel magnetic field. As seen in the preceding section, the subsequent behavior depends on the mechanism that produces the superflow, owing to different conserved quantities in a torus and in heat flow.

It is important to realize that other experimental situations also can lead to the formation of helical textures. Even in the absence of a magnetic field, for example, lowering the temperature can induce a helix because the hydrodynamic parameters are temperature dependent.[3,12] Figure 2 shows that the region I of stability for the uniform state shrinks with decreasing temperature, and its disappearance at $\approx 0.82 T_c$ indicates the spontaneous distortion to a helical texture for arbitrarily small v_0.

Once formed, by whatever mechanism, the helix can become unstable in many varied ways. For simplicity, we shall treat only the case of small-angle dipole-locked helices, where analytic expressions are readily available. In the case of heat flow, for example, the general region of stability for $\beta_0 \ll 1$ is given by

$$H^2 + v_0^2[(C_0 + \tfrac{1}{2})^2 (K_b^L)^{-1} - \rho_0] > 3K_b^L (u - u_h)^2 \ , \tag{76}$$

where u is the actual pitch of the helix, $u_h \equiv (C_0 + \frac{1}{2}) v_0 / K_b^L$, and v_0 is the initial relative superflow when the helix first forms. Note that the helix is stable for a range of pitches about the preferred value u_h, even though u is expected to retain the value u_h. Suppose, however, that the heat current changes after the helix is formed. The new value v_0' will produce a new preferred u_h' different from that appropriate to the original helix. Since a small value of $v_0 - v_0'$ can easily violate the inequality in Eq. (76), even a small alteration in the heat current can render the helix unstable. In addition, the preceding analysis of nonlinear growth beyond the threshold for instability remains correct, again implying a catastrophic transition to a new and qualitatively different regime. Similar considerations apply to a change in the temperature after the helix forms, for the temperature dependence[3,12] of the coefficient $(C_0 + \frac{1}{2})/K_b^L$ again alters the optimum value of the pitch even at fixed v_0.

An analogous calculation for a helix in a torus leads to a slightly different condition for stability, in that the right-hand side of Eq. (76) acquires an extra term $2\beta_0^2 H^4 / v_0^2$. Since this additional term is positive definite, small-angle helices in a torus should be more sensitive to changes in the optimum pitch than those produced by heat flow. It would be interesting to search for such an effect on a persistent current in a torus, where a magnetic field would produce a static helical texture. Torsional oscillations could modulate $v_{sz} - v_n$, which, in turn, should induce an instability of the helical texture at a critical amplitude. Such behavior could be monitored through a change in the nuclear magnetic resonance,[10,33] or, perhaps, directly as an altered current and angular momentum.

ACKNOWLEDGMENTS

We are grateful to D. J. Bromley and to B. A. Huberman for valuable discussions. This research

was supported in part by the National Science Foundation through Grant No. DMR 78-25258.

APPENDIX A: STABILITY OF UNIFORM TEXTURES

The basic dynamical relations are those in Eqs. (9)–(11) concerning the time dependence of $\hat{l}$, $\hat{d}$, and the local phase Φ. In the case of a large relative superflow $\vec{v}_s - \vec{v}_n = v_0\hat{z}$, and a small parallel magnetic field H, the initial uniform configuration has $\hat{l} = \hat{d} = \hat{z}$. To study the time dependence of small deviations, it is simplest to use Cartesian variables,[1] with

$$\hat{l} = \hat{z} + \delta\hat{l}, \quad \hat{d} = \hat{z} + \delta\hat{d}, \quad \Phi = -v_s z + \delta\Phi \ , \tag{A1}$$

where the small variations in $\hat{l}$ and $\hat{d}$ must satisfy the constraints $\hat{l}\cdot\hat{l} = 1$ and $\hat{d}\cdot\hat{d} = 1$. To second order in the small quantities, these conditions require

$$\begin{aligned} \delta\hat{l} &= \hat{x}\,\delta l_x + \hat{y}\,\delta l_y - \tfrac{1}{2}\hat{z}(\delta l_x^2 + \delta l_y^2) \ , \\ \delta\hat{d} &= \hat{x}\,\delta d_x + \hat{y}\,\delta d_y - \tfrac{1}{2}\hat{z}(\delta d_x^2 + \delta d_y^2) \ . \end{aligned} \tag{A2}$$

Moreover, since

$$\delta\hat{l} \approx \delta\beta(\hat{x}\cos\alpha + \hat{y}\sin\alpha) \tag{A3}$$

to leading order, and

$$\vec{v}_s = -\vec{\nabla}(\gamma + \delta\gamma) - \cos(\delta\beta)\vec{\nabla}(\alpha + \delta\alpha) \ , \tag{A4}$$

a simple analysis shows that $\delta\vec{v}_s$ can be expressed in terms of the Cartesian components[1]

$$\delta\vec{v}_s = \vec{\nabla}\delta\Phi + \tfrac{1}{2}(\delta l_x\vec{\nabla}\delta l_y - \delta l_y\vec{\nabla}\delta l_x) \tag{A5}$$

correct through second order, where $\delta\Phi \approx -(\delta\alpha + \delta\gamma)$.

Similar relations for $\hat{d}$ lead to five independent variables $\eta_\lambda \equiv \{\delta l_x, \delta l_y, \delta\Phi, \delta d_x, \delta d_y\}$ with $\lambda = 1, \ldots, 5$, and we therefore obtain a set of five coupled linearized equations whose coefficients are the second partial derivatives of the free-energy density with respect to these variables and their gradients. For example, the two independent components of Eq. (9) become ($\lambda = 1, 2$)

$$\mu\left(\frac{\partial}{\partial t} + v_n\frac{\partial}{\partial z}\right)\eta_\lambda = \left[\frac{\partial^2 f}{\partial(\nabla_i\eta_\lambda)\partial(\nabla_j\eta_\mu)}\nabla_i\nabla_j + \frac{\partial^2 f}{\partial(\nabla_i\eta_\lambda)\partial\eta_\mu}\nabla_i - \frac{\partial^2 f}{\partial\eta_\lambda\partial(\nabla_i\eta_\mu)}\nabla_i - \frac{\partial^2 f}{\partial\eta_\lambda\partial\eta_\mu}\right]\eta_\mu \ , \tag{A6}$$

where the partial derivatives are evaluated in the uniform texture; the corresponding three equations for $\delta\Phi, \delta d_x, \delta d_y$ ($\lambda = 3, 4, 5$) differ only in that the left-hand side is replaced by zero. It is convenient to expand all the small variations in Fourier series

$$\eta_\lambda(\vec{r}, t) = \sum_{\vec{k}} e^{i\vec{k}\cdot\vec{r} + \sigma t}\eta_{\lambda\vec{k}} \ , \tag{A7}$$

which leads to an algebraic equation for the quantity $\Omega = \sigma + i\vec{k}\cdot\vec{v}_n$. If $\mathrm{Re}\sigma$ is positive for any $\vec{k}$, then the configuration is unstable, whereas it is stable if $\mathrm{Re}\sigma$ is negative for all $\vec{k}$. There are, in fact, only two nontrivial degrees of freedom, and it is convenient to eliminate $\delta\Phi$ and $\delta\vec{d}$ in terms of δl_x and δl_y. The resulting eigenvalue equation has the form

$$\begin{aligned} (\Omega\mu + A)\delta l_x + B\,\delta l_y &= 0 \ , \\ B^*\delta l_x + (\Omega\mu + C)\delta l_y &= 0 \ , \end{aligned} \tag{A8}$$

where

$$\begin{aligned} A &= A(k_x, k_y, k_z) = 1 + \rho_0 v_0^2 + K_s k_x^2 + K_t k_y^2 + K_b k_z^2 - (\rho_s k^2 - \rho_0 k_z^2)^{-1}(C_0^2 k_y^2 k_z^2 + v_0^2\rho_0^2 k_x^2) \\ &\quad - [1 - H^2 + K_1 k_z^2 + K_2(k_x^2 + k_y^2)]^{-1} \ , \\ B &= [K_s - K_t - (\rho_s k^2 - \rho_0 k_z^2)^{-1}(v_0^2\rho_0^2 - C_0^2 k_z^2)]k_x k_y + i v_0 k_z[1 + 2C_0 - \rho_0 C_0(k_x^2 + k_y^2)(\rho_s k^2 - \rho_0 k_z^2)^{-1}] \ , \\ C &= A(k_y, k_x, k_z) \ . \end{aligned} \tag{A9}$$

Since the matrix of coefficients is Hermitian, the eigenvalues Ω_1 and Ω_2 are real, and the instability occurs when their product $AC - |B|^2$ vanishes. Thus the uniform texture is stable if

$$AC - |B|^2 > 0, \quad \forall\,\vec{k} \ . \tag{A10}$$

Numerical evaluation for various values of v_0 and H indicates that the instability first occurs for longitudinal fluctuations ($\vec{k} = k\hat{z}$), in which case $A = C$ and B is pure imaginary. The instability thus appears when

$$A - |B| = 0 \tag{A11a}$$

and

$$\frac{\partial}{\partial k}(A - |B|) = 0 \ . \tag{A11b}$$

Direct calculation yields the conditions

$$\rho_0 v_0^2 + K_b k^2 + (K_1 k^2 - H^2)(1 - H^2 + K_1 k^2)^{-1} = v_0 k (2C_0 + 1) \ , \quad \text{(A12a)}$$

$$[K_b + K_1 (1 - H^2 + K_1 k^2)^{-2}] k = v_0 (C_0 + \tfrac{1}{2}) \ . \quad \text{(A12b)}$$

It is not difficult to eliminate $1 - H^2 + K_1 k^2$ from these equations, whose solution then yields the critical wave number k_c for a given value of v_0, and the associated magnetic field. Figure 2 shows the corresponding stable region I for several temperatures. Near the origin ($v_0 \ll 1$, $H \ll 1$), the critical field has the analytic form given in Eq. (28a) with

$$k_c \approx (C_0 + \tfrac{1}{2}) v_0 / K_b^L \ , \quad \text{(A13)}$$

but the remaining portion requires numerical analysis. It is evident that the coefficients A, B, and C do not converge uniformly as $\vec{k} \to 0$. Indeed, the assumption[34] that $k = 0$ yields the less restrictive condition $v_0^2 > H^2 (1 - H^2)^{-1}$ for the stability of the uniform state with respect to uniform rotations of $\hat{l}$ and $\hat{d}$. Thus the inclusion of phase variations and the allowance for nonzero wave numbers considerably reduces the stability of the uniform texture $\hat{l} = \hat{d} = \hat{z}$.

A similar procedure determines the stability of region II of Fig. 2 ($\hat{l} = \hat{d} = \hat{x}$ in large field $H\hat{z}$ and small parallel relative superflow $v_0 \hat{z}$). The criterion (A10) remains correct, but with the coefficients now given by

$$A = K_s k_y^2 + K_t k_z^2 + K_b k_x^2 - (C_0 k_x k_z)^2 (\rho_s k^2 - \rho_0 k_x^2)^{-1} + 1 - [1 + K_1 k_x^2 + K_2 (k_y^2 + k_z^2)]^{-1} \ , \quad \text{(A14a)}$$

$$B = [K_s - K_t + C_0^2 k_x^2 (\rho_s k^2 - \rho_0 k_x^2)^{-1}] k_y k_z + i v_0 k_z [\rho_s - C_0 - \rho_0 C_0 k_x^2 (\rho_s k^2 - \rho_0 k_x^2)^{-1}] \ , \quad \text{(A14b)}$$

$$C = 1 - \rho_0 v_0^2 + K_s k_z^2 + K_t k_y^2 + K_b k_x^2 - k_x^2 (C_0^2 k_y^2 + \rho_0^2 v_0^2)(\rho_s k^2 - \rho_0 k_x^2)^{-1} - [1 + H^2 + K_1 k_x^2 + K_2 (k_y^2 + k_z^2)]^{-1} \ . \quad \text{(A14c)}$$

Once again, the most restrictive condition arises for $\hat{k} = \hat{l}$, but it now occurs as a long-wavelength instability with $k_y = k_z = 0$ and $k_x \to 0$; the associated boundary of region II (see Fig. 2) becomes[35]

$$v_c = \frac{1}{(\rho_0 \rho_s)^{1/2}} \frac{H}{(1 + H^2)^{1/2}} \ . \quad \text{(A15)}$$

This critical velocity has a characteristic dependence on magnetic field, which might be detectable experimentally.[36] The overall coefficient is $(\sqrt{2})^{-1}$ near T_c, but it has an unusual temperature dependence through ρ_0. Other choices for the direction of $\vec{k}$ yield less restrictive conditions; for example, the factor $(\rho_0 \rho_s)^{1/2}$ is replaced by $[\rho_0 + (\rho_s - C_0)^2 / (K_t + K_2)]^{1/2}$ if $k_x = k_y = 0$ and $k_z \to 0$, and by 1 if k is set equal to zero from the start.

APPENDIX B: EFFECT OF MODULATING THE MAGNETIC FIELD

Recent studies of harmonically forced one-dimensional motion in an anharmonic potential well[37] make it interesting to consider the effect of a small harmonic modulation of the magnetic field. For definiteness, we assume that $\vec{H}$ remains uniform and of the form

$$\vec{H} = H (1 + \epsilon \cos \omega t) \hat{z} \ , \quad \text{(B1)}$$

where $\epsilon \ll 1$. The formalism of Sec. IV is readily generalized to include this behavior. In particular, Eq. (52a) remains unchanged, but the right-hand side of Eq. (52b) acquires the extra terms

$$2\epsilon H^2 \cos\beta_0 \cos\omega t + \epsilon^2 H^2 [\tfrac{1}{2} \cos\beta_0 (1 + \cos 2\omega t) + 2y \cos 2\beta_0 \cos\omega t] + \cdots \ . \quad \text{(B2)}$$

Since H is uniform, these extra driving terms affect only the $m = 0$ components [see Eq. (54)] in lowest order, but the nonlinearities produce higher-order couplings that turn out to delay the instability of the helical texture from the value found in Secs. III and IV for $\epsilon = 0$.

To verify this assertion, it is helpful to expand the spatial Fourier coefficients $x_m(t)$ and $y_m(t)$ [see Eq. (54)] in a further Fourier series

$$x_m(t) = \sum_j x_{m,j} e^{-ij\omega t} \ , \quad y_m(t) = \sum_j y_{m,j} e^{-ij\omega t} \ , \quad \text{(B3)}$$

where $x_{m,j}$ and $y_{m,j}$ are constant coefficients (apart from those with $j = 0$, which may undergo slow variations relative to the period of the oscillatory field). Evidently, only the two terms $y_{0,1}$ and $y_{0,-1}$ are of order ϵ, and a simple calculation yields the explicit relations

$$y_{0,1} = \frac{\epsilon H^2 \cos\beta_0}{c + i\omega\mu} \ , \quad y_{0,-1} = \frac{\epsilon H^2 \cos\beta_0}{c - i\omega\mu} \ . \quad \text{(B4)}$$

The instability of the helix appears through the time dependence of the Fourier coefficients $x_{1,0}$ and $y_{1,0}$, which involve nonlinear terms of the typical form $y_{0,1} x_{1,-1}$, $y_{0,-1} x_{1,1}$ and other similar ones. Thus it also becomes necessary to consider the equations

for $x_{1,\pm1}$ and $y_{1,\pm1}$, which again involve nonlinear couplings, now of the form $y_{0,\pm1}x_{1,0}$ or $y_{0,\pm1}y_{1,0}$. Since $y_{0,\pm1}$ is known from Eq. (B4) to leading order in ϵ, these last equations are effectively linear and may be solved for $x_{1,\pm1}$ and $y_{1,\pm1}$ in terms of $x_{1,0}$ and $y_{1,0}$. Substituting back into the dynamical equations for $x_{1,0}$ and $y_{1,0}$ leads to a set of linear equations similar to those in Eq. (56), but whose coefficients have additional contributions of order ϵ^2. A lengthy calculation that works to zero order in k_0 and to first order in ϵ^2 yields the modified stability condition [compare Eq. (58) and the following discussion]

$$ac-b^2+\frac{2\epsilon^2H^4}{(\omega^2\mu^2+c^2)^2}\{b^2c^2\sin^4\beta_0-[(fc-bg)\cos\beta_0-bc\sin^2\beta_0]^2 + (\omega^2\mu^2+c^2)[b^2\cos2\beta_0-2\cos^3\beta_0(ce-bf)]\}=0 \ . \quad \text{(B5)}$$

Numerical evaluation shows that the factor in braces is positive at the original point of instability ($\epsilon=0$), both for a torus and for heat flow. Thus modulating the magnetic field actually stabilizes the helix because the quantity $ac-b^2$ must become negative definite before Eq. (B5) can be satisfied. The effect is largest at low frequencies and falls to zero when $\omega\mu >> c$. If the instability of the helical texture is eventually detected for a uniform static magnetic field, it would be interesting to investigate this nonlinear stabilization. In particular, the critical opening angle (see Table I) should increase by a term of order ϵ^2.

Similar calculations for a field of the form $H\hat{z}(1+\epsilon\cos k_0 z\cos\omega t)$ indicate that such a spatially varying perturbation has a destabilizing effect, in contrast to the situation for a uniform perturbation. Unfortunately, construction of this sort of field is likely to be difficult, so that experimental study of this latter configuration appears remote.

[1]P. Bhattacharyya, T.-L. Ho, and N. D. Mermin, Phys. Rev. Lett. 39, 1290 (1977).

[2]M. C. Cross and M. Liu, J. Phys. C 11, 1795 (1978).

[3]A. L. Fetter, Phys. Rev. Lett. 40, 1656 (1978); J. Phys. (Paris) 39, C6-46 (1978); Phys. Rev. B 20, 303 (1979).

[4]H. Kleinert, Y. R. Lin-Liu, and K. Maki, J. Phys. (Paris) 39, C6-59 (1978); Phys. Lett. 70A, 27 (1979).

[5]Y. R. Lin-Liu, K. Maki, and D. Vollhardt, J. Phys. (Paris) Lett. 39, 381 (1978).

[6]W. M. Saslow and C.-R. Hu, J. Phys. (Paris) Lett. 39, L-379 (1978).

[7]S. Takagi, Prog. Theor. Phys. (Kyoto) 60, 934 (1978).

[8]J. R. Hook and H. E. Hall, J. Phys. C 12, 783 (1979).

[9]Y. R. Lin-Liu, D. Vollhardt, and K. Maki, Phys. Rev. B 20, 159 (1979).

[10]D. Vollhardt, Y. R. Lin-Liu, and K. Maki, J. Low Temp. Phys. 37, 627 (1979).

[11]A. L. Fetter and M. R. Williams, Phys. Rev. Lett. 43, 1601 (1979).

[12]H. Kleinert, Phys. Lett. 71A, 66 (1979); in *New Aspects of Subnuclear Physics,* edited by A. Zichichi (Plenum, New York, 1980).

[13]S. Chandrasekhar, *Hydrodynamic and Hydromagnetic Stability* (Oxford University Press, London, 1961), Chaps. II and VII.

[14]L. D. Landau and E. M. Lifshitz, *Fluid Mechanics* (Pergamon, London, 1959), Chap. III and Sec. 56.

[15]R. P. Feynman, R. B. Leighton, and M. Sands, *The Feynman Lectures on Physics* (Addison-Wesley, Reading, Mass., 1964), Chap. 41.

[16]C. Normand, Y. Pomeau, and M. G. Velarde, Rev. Mod. Phys. 49, 581 (1977).

[17]A similar calculation in Ref. 9 differs from ours in allowing the pitch of the helix to change with increasing field. In contrast, we argue in Sec. III that the proper procedure is to hold the pitch constant. In addition, they consider only the case of constant current (heat flow) and require equal torsional motions for $\hat{d}$ and $\hat{l}$.

[18]T.-L. Ho, in *Quantum Fluids and Solids,* edited by S. B. Trickey, E. D. Adams, and J. W. Dufty (Plenum, New York, 1977), p. 97.

[19]C.-R. Hu and W. M. Saslow, Phys. Rev. Lett. 38, 605 (1977).

[20]W. F. Brinkman and M. C. Cross, in *Progress in Low Temperature Physics,* edited by D. J. Brewer (North-Holland, Amsterdam, 1978), Vol. VIIA, p. 105.

[21]We follow the notation and derivation of T.-L. Ho, Ph.D. thesis (Cornell University, 1978) (unpublished). In addition we use dimensionless variables, in which the hydrodynamic parameters are measured in units of $\bar{\rho}_{\parallel}\equiv\bar{\rho}_s-\bar{\rho}_0$, where bars denote the dimensional hydrodynamic parameters from the last of Ref. 3 (thus, for example, the dimensional total density is $\rho\bar{\rho}_{\parallel}$). Energy density is measured in units of the dipole coupling constant $\lambda_d\approx10^{-5}$ erg cm^{-3}, length is measured in units of $L^*=(\bar{\rho}_{\parallel}/\lambda_d)^{1/2}\approx6$ μm, and H is measured in units of $H^*=(\lambda_d/\lambda_m)^{1/2}\approx30$ Oe, where λ_m characterizes the alignment energy of the spin vector $\hat{d}$ in a magnetic field. Units of time are chosen so that $\hbar/2m_2=1$, and the orbital viscosity [see Eq. (9)] includes the factor λ_d^{-1} implicit in the dimensionless free-energy density.

[22]M. C. Cross, J. Low Temp. Phys. 21, 525 (1975).

[23]M. C. Cross and P. W. Anderson, in *Proceedings of the Fourteenth International Conference on Low Temperature Physics,* edited by M. Krusius and M. Vourio (North-Holland, Amsterdam, 1976), Vol. I, p. 29.

[24]H. Goldstein, *Classical Mechanics* (Addison-Wesley, Palo Alto, 1965), p. 219.

[25]The boundary conditions at $z=0$ and $z=L$ also require $\hat{l}$ to be perpendicular to the walls. If $L >> L^*$, however,

the additional bending energy of $\hat{l}$ near the boundaries can be ignored as a surface effect. Thus the only role of the boundaries is to set the z component of the current to zero.

[26]This configuration entails additional considerations and will be treated separately.

[27]The effect of transverse variations $\propto \exp i(k_x x + k_y y)$ has been treated in Ref. 3 for a dipole-locked system in zero field.

[28]This procedure is most intuitive for the case of a torus, but it also applies to an external heat flow if ζ is taken from Eq. (40b). Alternatively, the Routhian procedure [see Eq. (24)] eliminates γ entirely, leaving only four independent variables. For heat flow, the constant j_z^0 is independent of the point of instability, but it depends explicitly on β_0 and u_h for a torus. For the details of these calculations, see M. R. Williams, Ph.D. thesis (Stanford University, 1979) (unpublished).

[29]It is important to remember that only longitudinal fluctuations have been considered here; conceivably, wide-angle helices may be unstable with respect to more general small deformations.

[30]Formally, the (omitted) cubic corrections in Eq. (52) also contribute to the A^3 term, but they turn out to be of higher order in $k_0 a/b \ll 1$.

[31]These values have been recomputed and differ somewhat from those in Ref. 11.

[32]This behavior may explain the periodic precession observed by D. N. Paulson, M. Krusius, and J. C. Wheatley, Phys. Rev. Lett. 37, 599 (1976).

[33]D. J. Bromley, Phys. Rev. B 21, 2754 (1980).

[34]R. Kleinberg, J. Low Temp. Phys. 35, 489 (1979).

[35]A. L. Fetter, Phys. Rev. B 14, 2801 (1976).

[36]M. A. Paalanen and D. D. Osheroff, Phys. Rev. Lett. 45, 362 (1980).

[37]B. A. Huberman and J. P. Crutchfield, Phys. Rev. Lett. 43, 1743 (1979)